



Geophysical Research Letters*



RESEARCH LETTER

10.1029/2023GL105450

Key Points:

- We develop an adaptable statistical framework using radar sounding data to classify the basal thermal state of ice sheets
- Applied to the Adélie-George V
 Coast, the framework reveals a mix
 of frozen and thawed-bed, along with
 confidence in the classifications
- Areas maintaining the region's stability have varied thermal states and we consider how this could increase sensitivity to climate forcing

Supporting Information:

Supporting Information may be found in the online version of this article.

Correspondence to:

E. J. Dawson, ejdawson@stanford.edu

Citation:

Dawson, E. J., Schroeder, D. M., Chu, W., Mantelli, E., & Seroussi, H. (2024). Heterogeneous basal thermal conditions underpinning the Adélie-George V Coast, East Antarctica. *Geophysical Research Letters*, *51*, e2023GL105450. https://doi.org/10.1029/2023GL105450

Received 14 JUL 2023 Accepted 6 JAN 2024

© 2024 The Authors. This is an open access article under the terms of the Creative Commons Attribution-NonCommercial License, which permits use, distribution and reproduction in any medium, provided the original work is properly cited and is not used for commercial purposes.

Heterogeneous Basal Thermal Conditions Underpinning the Adélie-George V Coast, East Antarctica

Eliza J. Dawson¹, Dustin M. Schroeder^{1,2}, Winnie Chu³, Elisa Mantelli^{4,5}, and Helene Seroussi⁶

¹Department of Geophysics, Stanford University, Stanford, CA, USA, ²Department of Electrical Engineering, Stanford University, Stanford, CA, USA, ³School of Earth and Atmospheric Science, Georgia Institute of Technology, Atlanta, GA, USA, ⁴Alfred Wegener Institute for Polar and Marine Research, Bremerhaven, Germany, ⁵Department of Earth and Environmental Sciences, Ludwig-Maximillians-Universitaet, Munich, Germany, ⁶Thayer School of Engineering, Dartmouth College, Hanover, NH, USA

Abstract Adélie-George V Land in East Antarctica, encompassing the vast Wilkes Subglacial Basin, has a configuration that could be prone to ice sheet instability: the basin's retrograde bed slope could make its marine terminating glaciers vulnerable to warm seawater intrusion and irreversible retreat under predicted climate forcing. However, future projections are uncertain, due in part to limited subglacial observations near the grounding zone. Here, we develop a novel statistical approach to characterize subglacial conditions from radar sounding observations. Our method reveals intermixed frozen and thawed bed within 100 km of the grounding-zone near the Wilkes Subglacial Basin outflow, and enables comparisons to ice sheet model-inferred thermal states. The signs of intermixed or near thawed conditions raises the possibility that changes in basal thermal state could impact the stability of Adélie-George V Land, adding to the region's potentially vulnerable topographic configuration and sensitivity to ocean forcing driven grounding line retreat.

Plain Language Summary East Antarctica's Adélie-George V Land has been relatively stable over the last few decades. However, this region contains the Wilkes Subglacial Basin, which has a downward-sloping bed inland of the grounding zone. This could make irreversible retreat possible if warming seawater off the coast enters beneath the ice sheet. However, predicting the region's vulnerability is difficult, in part, because there is limited information about the conditions beneath the ice sheet. In this study, we develop a new statistical approach to synthesize radar sounding data and classify the conditions at the ice-bed interface into frozen-bed and thawed-bed, which can then provide comparisons to ice sheet model output. We find that areas near the outflow of the Wilkes Subglacial Basin, critical in maintaining the stability of the region, might consist of mixed frozen-bed and thawed-bed or near-thawed conditions on the scale of tens of kilometers across. This finding is important since the extent of basal thaw affects how easily ice can flow or slide over the bed. If parts of the bed are close to thawed, this could make Adélie-George V Land more sensitive to climate forcing, possibly resulting in mass loss.

1. Introduction

Adélie-George V Land in East Antarctica is an often overlooked candidate for major sea level contributions since it has experienced limited changes—roughly 0 Gt/yr mass balance over recent decades (Lovell et al., 2017; Rignot et al., 2019; Stokes et al., 2022). However, due to its retrograde bed configuration, this region has the potential to become a large source of East Antarctica mass loss if changing climate conditions bring warmer seawater onto the continental shelf (J. R. Jordan et al., 2023) where it could access the grounding zone causing irreversible retreat (Mengel & Levermann, 2014).

Wilkes Subglacial Basin holds most of the sea level rise potential of Adélie-George V Land. This broad, sedimentary basin extends almost 1,400 km inland (Figure 1a) and contains ice up to 3 km thick (Figure 1b), equating to 3–4 m of sea-level equivalent (Aitken et al., 2014; Ferraccioli et al., 2009; E. Rignot et al., 2019). This is similar in ice volume to the closely monitored Thwaites Glacier drainage basin in West Antarctica (Scambos et al., 2017). Wilkes Subglacial Basin has outlets in Cook and Ninnis glaciers along the George V Land Coast (Figures 1a–1d) (Rignot et al., 2011). Both glaciers have retrograde bed slopes (Morlighem et al., 2020) and are grounded below sea level (Constantino & Tinto, 2023) making them candidates for Marine Ice Sheet Instability (Mercer, 1978; Schoof, 2007). Furthermore, small volumes of ice, referred to as "ice plugs" (Figure 1d) could be

DAWSON ET AL. 1 of 12

19448007, 2024, 2, Downloaded from https://agupubs.onlinelibarry.wiley.com/doi/10.1029/2023GL105450 by Stanford University, Wiley Online Library on [03/04/2024]. See the Terms and Conditions (https://alimelibarry.wiley.com/kerms-and-conditions) on Wiley Online Library for rules of use; OA articles are governed by the applicable Creat

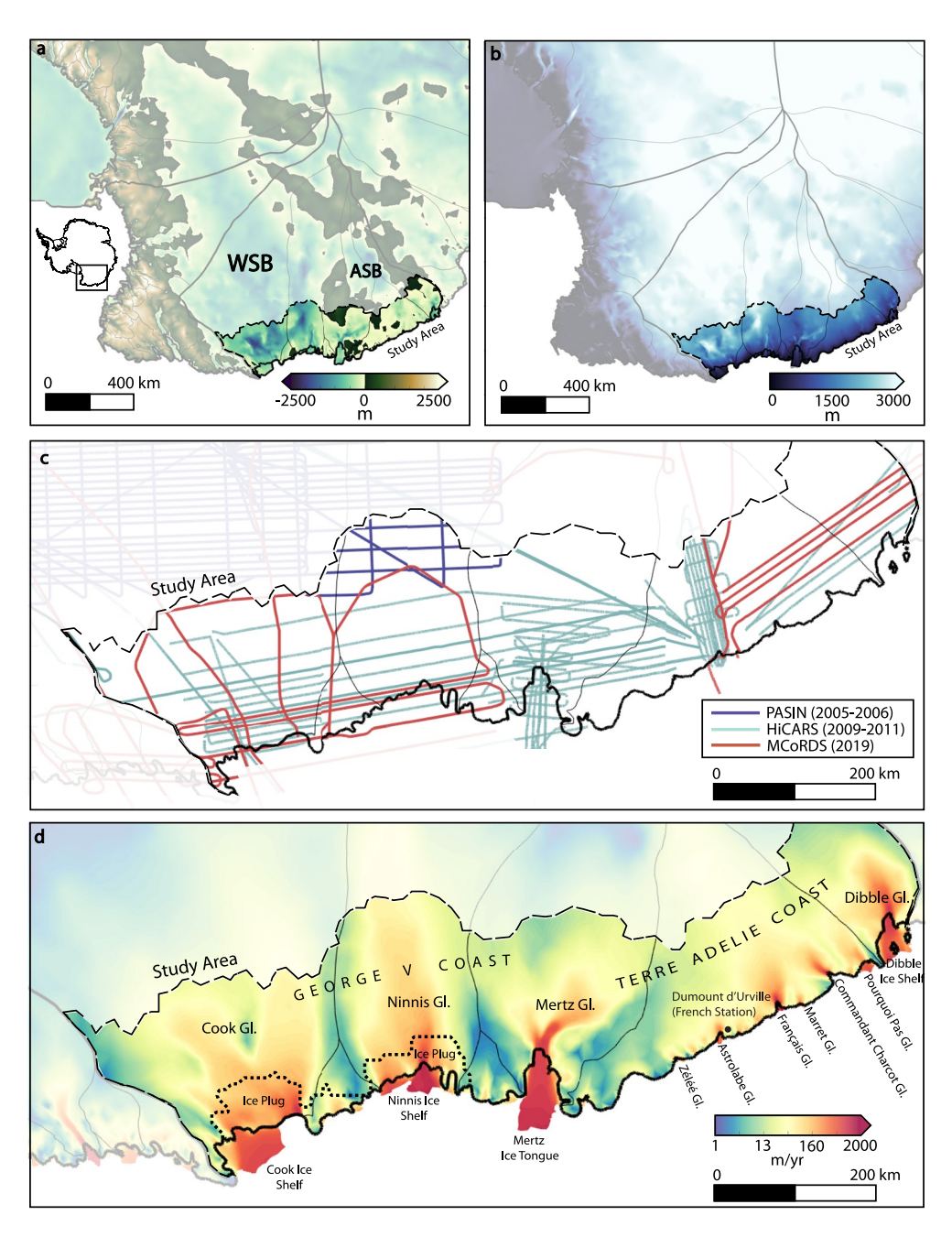


Figure 1. (a) Bed topography of Adélie-George V Land from BedMachine (Morlighem, 2022) with the dashed outline depicting the study area and labels indicating Wilkes Subglacial Basin (WSB) and Astrolabe Subglacial Basin (ASB), (b) Ice thickness of Adélie-George V Land from BedMachine (Morlighem, 2022), (c) Airborne ice-penetrating radar survey coverage in the Adélie-George V Land region, (d) Observed surface velocity from MEaSUREs InSAR-based Antarctic Version 2 velocity map (Mouginot et al., 2012; Rignot et al., 2011) with glacier locations labeled and the dotted line outlining ice plugs adapted from Mengel and Levermann (2014) Figure 2. The study area (dashed line) is defined as the zone of the D-D' region (The IMBIE team, 2018) that is within 100 km of fast flowing (>100 m/yr surface velocity) ice (following Dawson et al. (2022)).

the deciding factor for the stability of the marine-based ice, where previous work shows that eliminating the plugs results in self-sustaining retreat (Mengel & Levermann, 2014).

The ice shelves of Cook and Ninnis glaciers are currently in contact with relatively cold seawater (Adusumilli et al., 2020; Thompson et al., 2018), however paleo-marine sediment core records show evidence of significant retreat caused by warmer ocean temperatures in the past: during the Pliocene epoch \sim 4.8–3.5 mya, warm

DAWSON ET AL. 2 of 12

climatic intervals aligned with erosional evidence showing hundreds of kilometers of grounding line retreat (Cook et al., 2013). Also, during Marine Isotope Stages 11, 9, and 5—approximately 400, 330, and 125 kya respectively—geological evidence and sedimentology records show up to 700 km of retreat during interglacial periods with warmer Southern Ocean temperatures and elevated global mean sea level (Blackburn et al., 2020; Crotti et al., 2022). More recent satellite altimetry records between 1973 and 1989 capture the near complete breakup of Cook West Ice Shelf and upstream thinning 33 ± 12 cm/yr (Schröder et al., 2019), following oceanic warming in the middle of the 20th century. Collectively, this provides evidence that the Adélie-George V Coast grounding zone responds dynamically to sufficiently large climate and ocean perturbations.

Beneath the ice sheet, subglacial conditions also modulate ice flow in the Adélie-George V region. A 2006–2007 subglacial lake flood event in Wilkes Subglacial Basin has been linked to ice velocity increases of Cook East (Miles et al., 2018). Similarly, the presence of multiple subglacial lakes in the Terre-Adélie section and in the Astrolabe Subglacial Basin indicates basal ice at the pressure-melting point (Siegert & Glasser, 1997). Models show basal thermal conditions ranging from frozen to thawed bed across Adélie-George V Land, but are poorly constrained (Dawson et al., 2022; Pattyn, 2010; Wilch & Hughes, 2000). The basal thermal state is an important constraint since frozen bed conditions inhibit basal sliding, while basal temperatures at, or close to, the pressure melting point support the existence of subglacial water, basal sliding, and the formation of fast-flow of glaciers and ice streams (Kleiner & Humbert, 2014; Kyrke-Smith et al., 2014). The basal thermal state can also transition over time via thawing or refreezing (Engelhardt, 2004; Wilch & Hughes, 2000). While both basal thawing and refreezing can modulate ice flow, recent analysis shows that the effect of thawing could lead to significantly increased ice mass loss in Adélie-George V Land (Dawson et al., 2022). These findings suggest that the current ice configuration of the region could be sensitive to changes in subglacial conditions.

Limited model projections for Adélie-George V Land combined with insufficient observational constraints on the basal conditions along the coast, make it hard to accurately project the region's future evolution and potential contribution to sea level rise. In this study, we use radar sounding data to provide a first observationally based assessment of the englacial and subglacial configuration of the Adélie-George V Land coast (Figure 1). We focus our assessment on areas of the D-D' region (The IMBIE team, 2018) that are within 100 km of fast flowing ice because of the risk that basal thawing poses there (Dawson et al., 2022). Then we apply a novel logistic regression-based analytical approach based on the observed radar power to locate likely regions of frozen or thawed bed, an approach that can enable linkages from observational analysis to needed model constraints.

2. Radar Sounding Methods and Results

Airborne radar sounding data provides powerful observational constraints on subglacial environments (e.g., Bingham & Siegert, 2007; Dowdeswell & Evans, 2004; MacGregor et al., 2015; Matsuoka, Pattyn, et al., 2012; Schroeder et al., 2020). The radar signal energy encodes information about subglacial and englacial conditions, including englacial temperature and the thermal, material, and hydrologic condition of the bed via reflectivity and attenuation signals (Chu et al., 2021; MacGregor et al., 2015; Schroeder et al., 2020). As the radar signal propagates through the ice, it experiences attenuation losses depending on variations in ice temperature and chemistry, with higher attenuation rates through the warmer ice directly above the bed due to its exponential relationship with temperature (Matsuoka, MacGregor, & Pattyn, 2012). While englacial attenuation is often corrected for in radar analysis, it is also, itself, an indicator of temperature throughout the ice column with the highest attenuation rates from temperate ice above the bed (Jordan et al., 2016; Matsuoka, Pattyn, et al., 2012; Schroeder, et al., 2016). Additionally, the strength of the radar reflection from the ice-bed interface indicates the subglacial environment (Christianson et al., 2016; Peters, 2005). The reflection intensity is often interpreted in a relative sense and separated into two populations, where lower relative reflectivity indicates frozen dry bed conditions while higher relative reflectivity indicates thawed wet bed conditions (e.g., Chu et al., 2018; Oswald & Gogineni, 2012). Our study seeks to leverage these two temperature-dependent signals—depth average attenuation rate, and relative reflectivity—to empirically characterize the thermal state of the Adélie-George V coast.

2.1. Bed-Echo Power Extraction From Radar Sounding Data Sets

The Adélie George V Land region was surveyed by three radar sounding campaigns: (a) the British Antarctic Survey (BAS) Polarimetric radar Airborne Science Instrument (PASIN) with surveys spanning the 2005–2006

DAWSON ET AL. 3 of 12

19448007, 2024, 2, Downloaded from https://agupubs.onlinelibrary.wiley.com/doi/10.1029/2023GL105450 by Stanford University, Wiley Online Library on [03/04/2024]. See the Terms and Conditions (https://onlinelibrary.wiley

and-conditions) on Wiley Online Library for

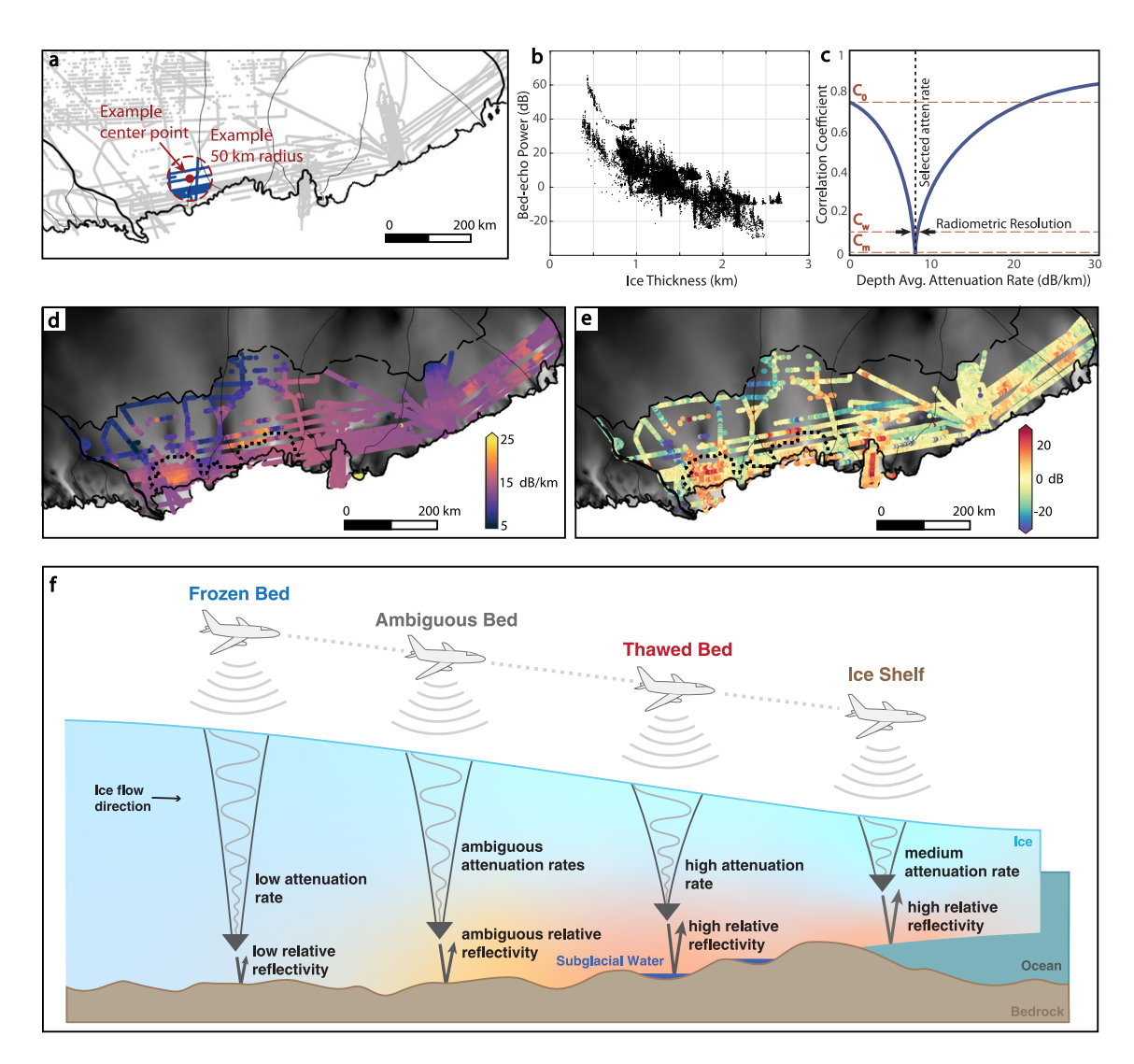


Figure 2. (a) Example center point and attenuation fitting radius for the 2d adaptive attenuation method. (b) Variation in ice thickness and bed-echo power within the example fitting radius. (c) Correlation coefficient from ice thickness and attenuation-corrected bed-echo power as a function of the attenuation rate for the example center point. C_0 is the correlation coefficient magnitude without correction, C_w is the correlation coefficient magnitude at which the radiometric resolution requirement is assessed, and C_m is the minimum correlation coefficient requirement, and identifies the attenuation rate fit (adapted from Schroeder et al. (2016)). (d) Map of bed-echo derived depth averaged attenuation rates (processed with a radiometric resolution requirement of 1 dB/km) for Adélie-George V Land with a background surface velocity map (Mouginot et al., 2012; Rignot et al., 2011) in gray scale, dotted outlines for the locations of ice plugs (Mengel & Levermann, 2014), and dashed outline showing the study area. (e) Corresponding relative reflectivity map. (f) Illustration showing relationship between radar attenuation rate and bed reflectivity, and the basal thermal state.

austral summer (Ferraccioli et al., 2021), (b) the University of Texas Institute for Geophysics (UTIG) High Capability Airborne Radar Sounder 1 and 2 (HiCARS) with surveys spanning the 2009–2011 austral summers (Blankenship, Kempf, Young, Richter, Schroeder, Greenbaum, et al., 2017; Blankenship, Kempf, Young, Richter, Schroeder, Ng, et al., 2017), and (c) the University of Kansas Center for Remote Sensing and Integrated Systems (CReSIS) Multichannel Coherent Radar Depth Sounder 3 (MCoRDS) with surveys over the 2019 austral summer (Hale et al., 2016). The surveys are shown in Figure 1c, and the radar system metrics are provided in Table S1 in Supporting Information S1.

Our first step is to calculate the bed-echo power using the unfocussed Synthetic Aperture Radar (SAR) (Peters et al., 2007) products from PASIN, HiCARS 1 and 2, and MCoRDS 3. This is done by extracting the peak power within a moving window around the bed picks published with the radar surveys. Then we combine the bed-echo power measurements from all surveys, following Chu et al. (2021) and Culberg et al. (2021), to reconcile radar system differences with cross-leveling (Figure S1 in Supporting Information S1). This results in a data set with a

DAWSON ET AL. 4 of 12

total of \sim 800,000 bed-echo power measurements, \sim 35,000 of which fall within the Adélie-George V Coast study area (see Figure 1c).

2.2. Attenuation Rate Calculation

Our study area has widely varying ice thickness and bed-echo power (example in Figures 2a and 2b) making our region well suited for deriving englacial attenuation rates from bed-echo power following the adaptive empirical fitting approach developed in 1D by Schroeder et al. (2016) and extended to 2D cross-profile analysis by Chu et al. (2021). The strength of this method is its ability to constrain spatial variations in englacial temperature at the glacier-catchment scale, captured in the depth average attenuation signal (Schroeder et al., 2016). However, to accurately estimate the attenuation rate, this method requires that the survey region has sufficient variation in ice thickness and bed-echo power within a fitting radius (Jacobel et al., 2010) (see Figures 2a and 2b).

Applying the 2D method, we select data points within an expanding radius (Figure 2a) until three goodness of fit conditions are met: (a) the initial magnitude of the correlation coefficient between ice thickness and bed-echo power is $C_0 \ge 0.7$, (b) the minimum correlation, $C_m \le 0.01$, and (c) the required radiometric resolution is achieved at the width where the minimum is assessed, $C_w = 0.1$ (see Figure 2c), following Chu et al. (2021) and Schroeder et al. (2016). We calculate attenuation rates using radiometric resolution requirements of both 1 dB/km and 2 dB/km to explore the sensitivity of the attenuation estimates to the radiometric resolution of the radar sensors (Schroeder et al., 2016). This attenuation fitting method is repeated for each data point in the study area, discarding points where the fitting conditions are not satisfied (more on the method in Text S1 and Figure S2 in Supporting Information S1).

2.3. Relative Reflectivity Calculation

Finally, we calculate bed reflectivity using the radar equation, which is expressed in the decibel scale as (Matsuoka, MacGregor, & Pattyn, 2012):

$$[P]_{dB} = [S]_{dB} - [G]_{dB} + [R]_{dB} - [L]_{dB} - [B]_{dB}$$
(1)

where $[P]_{dB}$ is the measured bed-echo power, $[S]_{dB}$ is the system parameters (calculated following Chu et al., 2021), $[G]_{dB}$ is the geometric spreading loss (calculated following Haynes et al., 2018), $[R]_{dB}$ is the bed reflectivity, $[L]_{dB}$ is the englacial attenuation (calculated using methods in Section 2.2), and $[B]_{dB}$ is birefringence losses, which we neglect (Chu et al., 2021). We then calculate relative reflectivity, $[R_{re}]_{dB}$, as expressed in Equation 2:

$$[R_{\rm rel}]_{\rm dB} = [R]_{\rm dB} - \text{mean}([R]_{\rm dB})$$
(2)

where we subtract the local bed reflectivity, $[R]_{dB}$, from the mean over the study area.

2.4. Attenuation Rate and Relative Reflectivity Results

Our map of attenuation rates reveal variation across the Adélie-George V Land coast on the scale of tens of kilometers (Figure 2d), while variation in relative reflectivity is finer scale (Figure 2e). The patterns are consistent with heterogeneous basal thermal conditions (Christianson et al., 2016; Chu et al., 2018). Lower attenuation rates and relative reflectivity values (~5 dB/km and -15--25 dB respectively, see Figures 2d and 2e) are generally observed in the ice sheet interior and in slow moving areas between glaciers as expected for cold-dry-bed regions (Matsuoka, MacGregor, & Pattyn, 2012). In contrast, the fast-flowing main trunks of Cook and Ninnis glaciers have the highest attenuation rates (up to 25 dB/km) and relative reflectivity values (up to 30 dB), indicative of thawed-wet-bed conditions. In between the ice sheet interior and margin and between fast flowing glaciers, we find more intermediate attenuation rates and intermixed relative reflectivity values, leading to a more ambiguous thermal state interpretation. Figure 2f illustrates the general attenuation rate and relative reflectivity pattens for various basal thermal states.

3. Logistic Regression-Based Classification of the Basal Thermal State

To overcome the qualitative ambiguity in interpreting attenuation rate and relative reflectivity, we design a new quantitative statistical framework. Our method uses binary logistic regression models (McCullagh & Nelder, 1989, Ch 4) and the basal thermal signatures encoded in the radar data to predict the likelihood of a frozen or thawed bed. Our study area contains patches of frozen and thawed bed to use as labeled training regions and we use the radar derived attenuation rate, relative reflectivity, and ice thickness as predictors. We include ice thickness as

DAWSON ET AL. 5 of 12

a predictor to account for its potential impact on the relationship between attenuation rate and relative reflectivity. For any given measurement location, a trained logistic regression model takes the three predictors as input and produces a prediction between 0 (frozen-bed) and 1 (thawed-bed). Then we linearly interpolate between all measurement locations to generate a continuous prediction map and bin it into classifications of frozen or thawed. Thermal state classifications from a single logistic regression model depend on the radar data used as predictors, the regions chosen as labeled training data, and the thresholds chosen to bin the predictions into thermal state classifications. We design a framework to be robust to these sensitivities.

Using a set of logistic regression models with different combinations of radar data processing and training data labeling, our method is robust to uncertainty in data preprocessing and training regions (Figure 3a; Table S2 in Supporting Information S1). With respect to data preprocessing, the strictest requirement is the radiometric resolution in the 2d attenuation fitting method. We processed data with 1 dB/km radiometric resolution as described in Section 2.2, and a more relaxed 2 dB/km (Figure S3 in Supporting Information S1 shows attenuation rates and relative reflectivity from the 2 dB/km requirement). The relative reflectivity and attenuation rates from both processing variations are used as predictors for logistic regression models. With respect to labeled training data, we use observed surface velocities to identify the fastest flowing regions in the study area, constituting parts of glaciers where basal sliding and a thawed bed is expected, and the slowest flowing regions constituting ice ridges where a frozen bed is expected. To be robust, the training data is chosen using both strict and relaxed thresholds for surface velocities. The strict thresholds are the fastest 10% and slowest 10% of surface velocities, while the relaxed thresholds are the fastest 15% and slowest 15% of surface velocities (Figure S5 in Supporting Information S1). We train logistic regression models with each combination of predictors and labeled data, resulting in four models with subsequent predictions for all measurement locations (Figure 3a).

Next, we interpolate the predictions and apply both strict and relaxed bounds for binning the predictions into thermal state classifications, yielding eight total realizations (Figure 3b). As a relaxed binning threshold, we use <0.4 to define frozen-bed and >0.6 to define thawed bed; for a stricter binning threshold, we use <0.3 and >0.7. Then, the realizations are stacked to show the thermal state classifications and agreement across realizations (Figure 3c).

To assess performance, each logistic regression model is evaluated against a common validation set—a subset of the labeled data omitted from training. The validation set assesses regression performance by comparing known labels with predictions, with metrics provided in Table S4 in Supporting Information S1. Coefficients for each predictor are also evaluated using maximum likelihood estimation to quantify their individual influence on the likelihood of a frozen or thawed bed and each predictor has an influence within one order of magnitude of each other, with relative reflectivity having the most influence in our study area (Figure S7 in Supporting Information S1). Finally, running a p-test shows that, for all models, all three predictors are statistically significant for predicting the basal thermal state, with *p*-values <0.05 (Table S5 in Supporting Information S1).

4. Discussion

Our synthesis of the basal thermal state shows interleaved frozen and thawed bed conditions on the order of tens of kilometers, across the study area (Figure 3c). Agreement across more regression realizations represents higher confidence thawed and frozen bed regions. High confidence thawed-bed predictions are found in parts of Cook Glacier, Mertz Glacier, and other smaller glaciers along the Terre-Adélie coast (Figure 3c). There are also interspersed high confidence frozen-bed patches west of Cook glacier, between Cook and Ninnis glaciers, and extending toward the interior. However, a majority of the study area has either lower confidence classifications, overlapping classifications, or no classification (see Figure 3c), which also provides useful information about the basal thermal conditions.

There are multiple scenarios that could produce intermediate predictions (close to 0.5). This could come from regions where the bed is near-thawed (Dawson et al., 2022; Mantelli & Schoof, 2019) or intermixed frozen and thawed-bed patches below the resolution of the radar observations (Chu et al., 2018). Alternatively, predictions near 0.5 could be from unclear attenuation rates, relative reflectivity, or ice thickness, resulting from unresolved ice sheet geometry, radar processing, or insufficient observations. Distinguishing between these scenarios will require ancillary information about the basal conditions in the lower confidence regions to update parameter ranges in labeling, radiometric resolution, and thresholding to refine classifications.

If the lower confidence classifications are interpreted as near thawed or intermixed frozen and thawed bed patches, this has implications for the stability of George V Land. The ice plugs—regions that have been previously identified as critical in maintaining the stability of Wilkes Subglacial Basin (Mengel & Levermann, 2014)—show

DAWSON ET AL. 6 of 12

19448007, 2024, 2, Downloaded from https://gappubs.onlinelibrary.wiley.com/doi/10.1029/2023GL105450 by Stanford University, Wiley Online Library on [03/04/2024]. See the Terms and Conditions (https://onlinelibrary.wiley.com/rerms-and-conditions) on Wiley Online Library for rules of use; OA articles are governed by the applicable Creativity

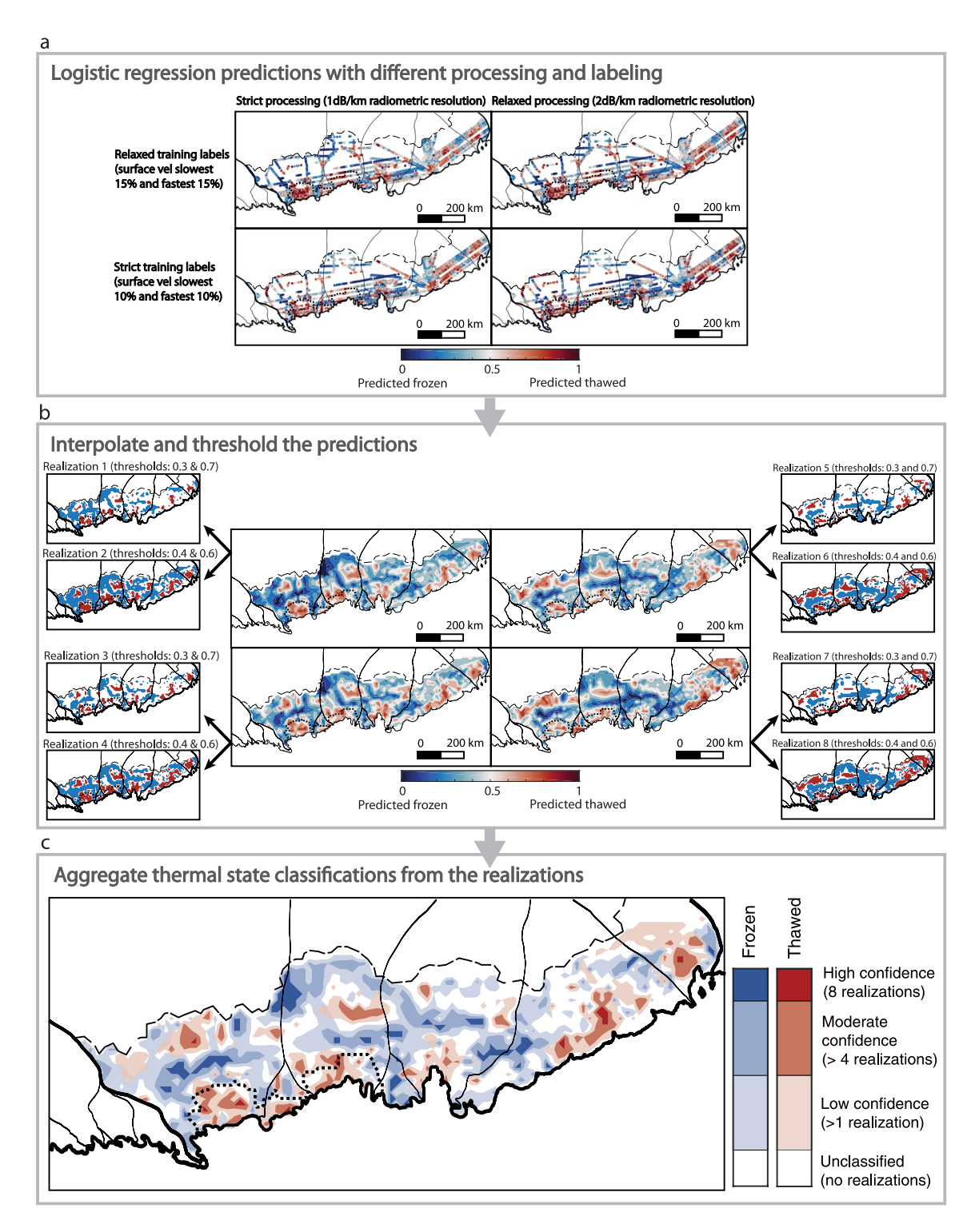


Figure 3. (a) Maps showing basal thermal state predictions along the radar lines from logistic regression models using different combinations of labeling and radar processing. (b) Central four maps display the entire study area's thermal state classifications from contouring the radar line predictions; eight realization maps reveal frozen-bed and thawed-bed classifications post-thresholding. (c) An aggregated map of frozen-bed and thawed-bed classifications (blue vs. red) displays agreement across eight realizations (shading from light to dark). The dotted outline indicates ice plug locations and dashed outline shows the study area.

DAWSON ET AL. 7 of 12

low-to-high confidence thawed bed classifications. This transitions to low-to-high confidence frozen bed classifications inland of the ice plugs (see Figure 3c). While some of the ice plug area intersects with labeled training regions (Figure S5 in Supporting Information S1) limiting the interpretability within those areas, heterogeneous or near-thawed basal thermal conditions could imply sensitivity thawing leading to ice mass loss (Dawson et al., 2022). This risk makes it pertinent to further investigate if the ice plugs could experience basal thawing, such as via warm seawater intrusion or increased frictional heating.

Our basal thermal state analysis is also comparable to ice sheet model output. While our framework outputs binary classifications and ice sheet models use discrete temperature fields, the classifications offer observational validation for model temperatures that are at, near, or below the pressure melting point (Figure 4). For example, most of the model-inferred thermal states (Dawson et al., 2022; Seroussi et al., 2020) also show near thawed to thawed conditions in the ice plug regions (Figure 4). However, the model-inferred thermal states tend to have larger extents of thawed-bed conditions extending inland of the ice plugs. This could mean that the processing, labeling, and thresholding bounds we use in our framework are overly cautious and more of the radar-inferred low confidence thawed bed regions would be classified as high confidence with tighter bounds. It is also possible that the discrepancy between radar observations and ice sheet modeling reveals a modeling bias inland of the ice plugs. The spread in model results can partially be attributed to different model initialization procedures, simulation purposes, and resolutions (Dawson et al., 2022; Seroussi et al., 2020), but should nonetheless be investigated to improve understanding of the thermal state.

More broadly, our analysis highlights the need for robust measurements of basal conditions that are useable for constraining ice sheet models. In thermally complex regions like the Adélie-George V Coast, resolving the subglacial and englacial thermal state matters for accurately projecting mass loss and sea level rise (Dawson et al., 2022). However, observations of the basal thermal state have not existed at the domain size and resolution needed to constrain ice sheet models. Our radar-derived thermal state classifications provide advancements toward bridging this gap. While our study area is a relatively small region, ongoing efforts to combine and increase radar-sounding data coverage of Antarctica could make constraints across a larger scale or even ice-sheet wide viable. Bringing observations to the point that they provide useable model constraints is key to enabling further ice sheet model development.

Beyond data and model development, information can be gained from using existing ice sheet model simulations and observations in unison. Observationally derived thermal state classifications can serve as a benchmark to assess large scale model-inferred conditions or perhaps even the ability of smaller scale physics-based models to capture thermo-mechanical processes (Mantelli et al., 2019). Additionally, sensitivity experiments comparing initialization procedures (Reese et al., 2020) and boundary conditions (Seroussi et al., 2017), or ensemble runs (Pittard et al., 2022; Pollard et al., 2016) could be expanded further using existing models.

Our logistic regression framework was developed to be applicable across a wide range of regions and scientific applications. To produce meaningful binary classifications, preexisting knowledge is needed for defining a subset of labeled data for training that is large enough to capture the statistical relationship between the input data and output predictions. The geophysical data sets used as predictors should be evaluated in terms of their statistical significance and individual influences on the predictions. It is also important to make sure the classes are balanced in quantity within the training set. With this is mind, the framework could be applied to other regions with similar conditions to distinguish frozen and thawed bed patches, though choosing bounds for processing, labeling, and thresholding would need to be updated for the new region. The framework could also be applied to focused data (Heliere et al., 2007; Peters et al., 2007) or other types of ice penetrating radar data (Schlegel et al., 2023), or used to classify other subglacial environments including grounding zone locations or subglacial lake detection. Additionally, the framework's ability to assess uncertainty could be further exploited, either by tracing individual influences from subsampling existing surveys or adding synthetic data. Uncertainty quantification could identify valuable regions for further geophysical surveying and accommodate future advancements in instrumentation and processing approaches (Broome et al., 2021; Hills et al., 2020).

5. Conclusions

In this analysis, we present new observationally derived constraints on the basal thermal conditions along the Adélie-George V Land coast along with levels of confidence in the thermal state classifications assigned by our logistic regression framework. We find a range of basal conditions including high confidence thawed-bed patches beneath fast flowing glaciers and high confidence frozen-bed along ice divides. Most notably, near the outlets of

DAWSON ET AL. 8 of 12

19448007, 2024, 2, Downloaded from https://agupubs.onlinelibrary.wiley.com/doi/10.1029/2023GL105450 by Stanford University, Wiley Online Library on [03/04/2024]. See the Terms and Conditions (https://onlinelibrary.wiley.com/rems-and-conditions) on Wiley Online Library for rules of use; OA articles are governed by the applicable Creative

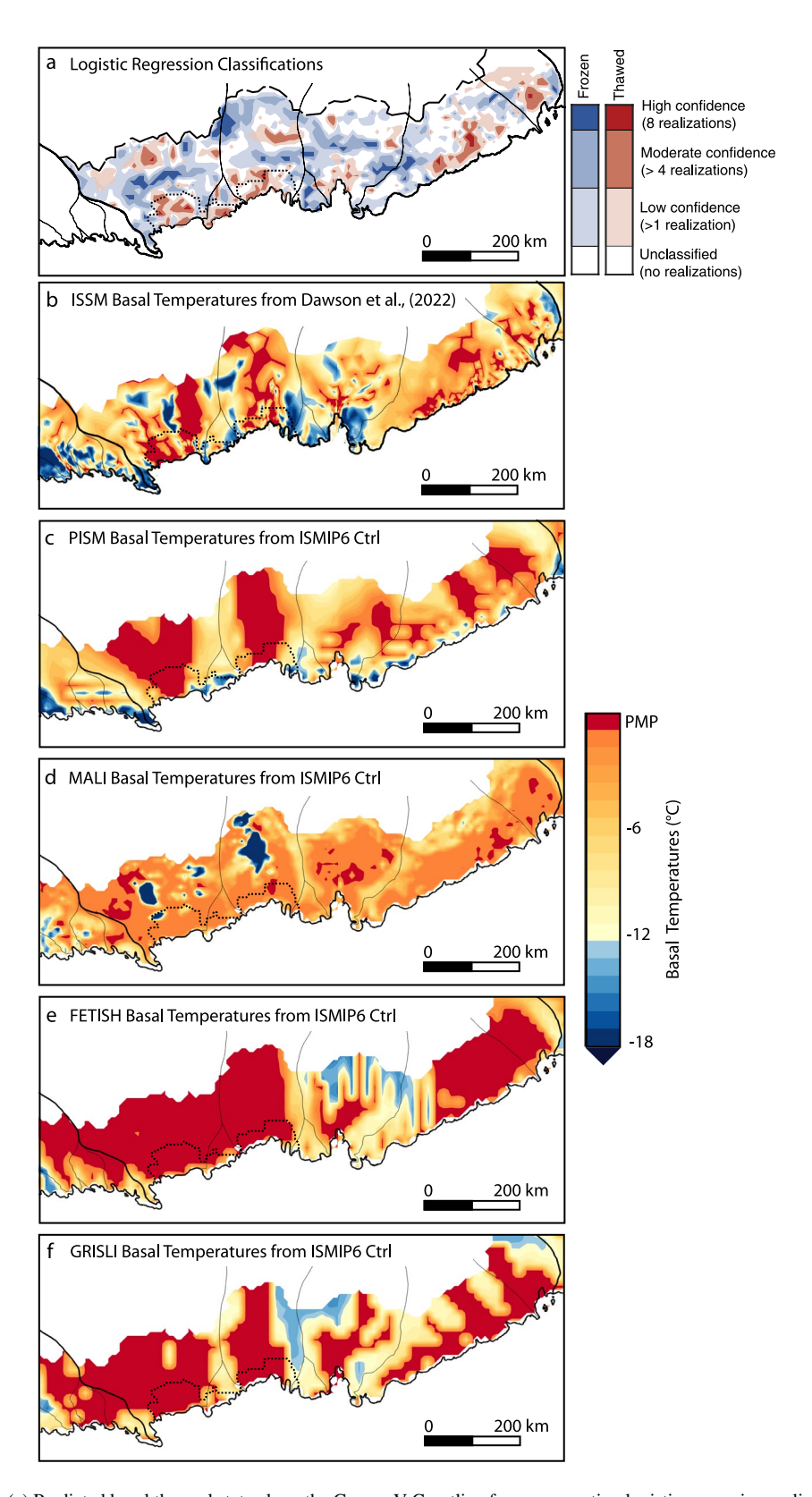


Figure 4. (a) Predicted basal thermal state along the George V Coastline from aggregating logistic regression realizations. (b) Pressure adjusted basal temperature derived using ISSM from Dawson et al. (2022). (c–f) Pressure adjusted basal temperatures from a subset of ice flow model output from the ISMIP6 control experiments (Seroussi et al., 2020).

DAWSON ET AL. 9 of 12

the Cook and Ninnis glaciers and extending inland, our results show lower confidence thawed-bed and frozen-bed classifications. This could represent highly intermixed frozen-bed and thawed-bed patches or an intermediate state that is frozen but close to thawing. Our basal thermal state classifications have the benefit of being comparable to thermal states inferred from ice sheet models, which show varying near thawed or intermixed frozen and thawed conditions. A heterogenous basal thermal state has the potential to be more sensitive to future climate forcing and just a small increase in basal temperatures could result in more thawed-bed regions, thereby accelerating ice flow and mass loss from Adélie-George V Land. Our evidence for especially heterogenous basal thermal conditions adds to previous findings that the region could be sensitive to the removal of ice plugs (Mengel & Levermann, 2014; Miles et al., 2018), ocean forcing driven grounding line retreat (J. R. Jordan et al., 2023), and basal thermal state (Dawson et al., 2022). Taken together, these components will likely determine how the Adélie-George V region responds to changes in the climate system.

Data Availability Statement

The processed data and logistic regression analysis results from this study are available on Zenodo (Dawson, 2023). The SAR processed radar sounding data sets used by this study are all freely downloadable from their respective sources. MCoRDS data can be downloaded from the CReSIS website (CReSIS, 2021). HiCARS data can be downloaded from the National Snow and Ice Data Center archive (Blankenship, Kempf, Young, Richter, Schroeder, Greenbaum, et al., 2017; Blankenship, Kempf, Young, Richter, Schroeder, Ng, et al., 2017), and can be searched and visualized on the Operation IceBridge Data Portal by filtering for the IceBridge HiCARS 1 L1B Time-Tagged Echo Strength Profiles V001 and IceBridge HiCARS 2 L1B Time-Tagged Echo Strength Profiles V001 surveys from 2009 to 2011 that cover the Adélie-George V Land study area. The PASIN data is the WISE-ISODYN survey (Ferraccioli et al., 2021), which can be accessed through the Airborne Geophysics Data Portal. The bed topography and ice thickness maps are available on the National Snow and Ice Data Center under MEaSUREs BedMachine Antarctica, Version 3 (Morlighem, 2022) and the MEaSUREs InSAR-based Antarctic Version 2 velocity map (Mouginot et al., 2012; Rignot et al., 2011; E. J. Rignot et al., 2017). The thermal model output from Dawson et al. (2022) can be accessed through Zenodo (Dawson, 2022), and the ISMIP6 thermal model output is also available on Zenodo (Seroussi, 2019).

Acknowledgments

E.D. was supported by the NSF GRFP under Grant DGE-1656518. D.M.S was supported by NASA Grant NNX16AJ95G and the NSF Grant 1745137. H.S. was supported by a grant from NASA Cryospheric Science Program (80NSSC22K0383). E.M. is Funded/ Co-funded by the European Union (ERC, PHAST, project number 01076793). Views and opinions expressed are those of the authors and do not necessarily reflect those of the European Union or the European Research Council. We acknowledge the use of data repositories from CReSIS, UTIG and BAS. We thank Riley Culberg for providing resources and advice on the radar processing analysis and Stuart Farris for offering helpful discussion. We also gratefully acknowledge the comments and advice from Editor Harihar Rajaram, as well as Ben Hills and an anonymous reviewer.

References

- Adusumilli, S., Fricker, H. A., Medley, B., Padman, L., & Siegfried, M. R. (2020). Interannual variations in meltwater input to the Southern Ocean from Antarctic ice shelves. *Nature Geoscience*, 13(9), 616–620. Article 9. https://doi.org/10.1038/s41561-020-0616-z
- Aitken, A. R. A., Young, D. A., Ferraccioli, F., Betts, P. G., Greenbaum, J. S., Richter, T. G., et al. (2014). The subglacial geology of Wilkes Land, East Antarctica. *Geophysical Research Letters*, 41(7), 2390–2400. https://doi.org/10.1002/2014GL059405
- Bingham, R. G., & Siegert, M. J. (2007). Radio-echo sounding over polar ice masses. *Journal of Environmental & Engineering Geophysics*, 12(1), 47–62. https://doi.org/10.2113/JEEG12.1.47
- Blackburn, T., Edwards, G. H., Tulaczyk, S., Scudder, M., Piccione, G., Hallet, B., et al. (2020). Ice retreat in Wilkes basin of East Antarctica during a warm interglacial. *Nature*, 583(7817), 554–559. https://doi.org/10.1038/s41586-020-2484-5
- Blankenship, D. D., Kempf, S. D., Young, D. A., Richter, T. G., Schroeder, D. M., Greenbaum, J. S., et al. (2017). IceBridge HiCARS 1 L1B time-tagged echo strength profiles, version 1 [Dataset]. NASA National Snow and Ice Data Center Distributed Active Archive Center. https://doi.org/10.5067/W2KXX0MYNJ9G
- Blankenship, D. D., Kempf, S. D., Young, D. A., Richter, T. G., Schroeder, D. M., Ng, G., et al. (2017). IceBridge HiCARS 2 L1B time-tagged echo strength profiles, version 1 [Dataset]. NASA National Snow and Ice Data Center Distributed Active Archive Center. https://doi.org/10.5067/017PFBVQOGO5
- Broome, A. L., Schroeder, D. M., & Johnson, J. T. (2021). Measuring englacial temperatures with a combined radar-radiometer. 2021 IEEE International Geoscience and Remote Sensing Symposium IGARSS, 2947–2950. https://doi.org/10.1109/IGARSS47720.2021.9554375
- Christianson, K., Jacobel, R. W., Horgan, H. J., Alley, R. B., Anandakrishnan, S., Holland, D. M., & DallaSanta, K. J. (2016). Basal conditions at the grounding zone of Whillans Ice Stream, West Antarctica, from ice-penetrating radar. *Journal of Geophysical Research: Earth Surface*, 121(11), 1954–1983. https://doi.org/10.1002/2015JF003806
- Chu, W., Hilger, A. M., Culberg, R., Schroeder, D. M., Jordan, T. M., Seroussi, H., et al. (2021). Multisystem synthesis of radar sounding observations of the Amundsen Sea sector from the 2004–2005 field season. *Journal of Geophysical Research: Earth Surface*, 126(10), e2021JF006296. https://doi.org/10.1029/2021JF006296
- Chu, W., Schroeder, D. M., Seroussi, H., Creyts, T. T., & Bell, R. E. (2018). Complex basal thermal transition near the onset of Petermann Glacier, Greenland. *Journal of Geophysical Research: Earth Surface*, 123(5), 985–995. https://doi.org/10.1029/2017JF004561
- Constantino, R. R., & Tinto, K. J. (2023). Cook ice shelf and Ninnis glacier tongue bathymetry from inversion of operation ice bridge airborne gravity data. Geophysical Research Letters, 50(11), e2023GL103815. https://doi.org/10.1029/2023GL103815
- Cook, C. P., Van De Flierdt, T., Williams, T., Hemming, S. R., Iwai, M., Kobayashi, M., et al. (2013). Dynamic behaviour of the East Antarctic ice sheet during Pliocene warmth. *Nature Geoscience*, 6(9), 765–769. https://doi.org/10.1038/ngeo1889
- CReSIS (2021). L1B geolocated radar echo strength profile data (2019 Antarctica GV). Digital Media. Retrieved from https://data.cresis.ku.edu/data/rds/2019_Antarctica_GV/CSARP_qlook/

DAWSON ET AL. 10 of 12

- Crotti, I., Quiquet, A., Landais, A., Stenni, B., Wilson, D. J., Severi, M., et al. (2022). Wilkes subglacial basin ice sheet response to Southern Ocean warming during late Pleistocene interglacials. *Nature Communications*, 13(1), 5328. https://doi.org/10.1038/s41467-022-32847-3
- Culberg, R., Schroeder, D. M., & Chu, W. (2021). Extreme melt season ice layers reduce firn permeability across Greenland. *Nature Communications*, 12(1), 2336. Article 1. https://doi.org/10.1038/s41467-021-22656-5
- Dawson, E. J. (2022). ISSM results for Antarctic ice sheet basal Thaw experiments [Dataset]. Zenodo. https://doi.org/10.5281/zenodo.6870567
- Dawson, E. J. (2023). Supporting data—Heterogeneous basal thermal conditions underpinning the Adélie-George V Coast, East Antarctica [Dataset]. Zenodo. https://doi.org/10.5281/zenodo.10445768
- Dawson, E. J., Schroeder, D. M., Chu, W., Mantelli, E., & Seroussi, H. (2022). Ice mass loss sensitivity to the Antarctic ice sheet basal thermal state. *Nature Communications*, 13(1), 4957. Article 1. https://doi.org/10.1038/s41467-022-32632-2
- Dowdeswell, J. A., & Evans, S. (2004). Investigations of the form and flow of ice sheets and glaciers using radio-echo sounding. *Reports on Progress in Physics*, 67(10), 1821–1861. https://doi.org/10.1088/0034-4885/67/10/R03
- Engelhardt, H. (2004). Thermal regime and dynamics of the West Antarctic ice sheet. Annals of Glaciology, 39, 85–92. https://doi.org/10.3189/172756404781814203
- Ferraccioli, F., Armadillo, E., Jordan, T., Bozzo, E., & Corr, H. (2009). Aeromagnetic exploration over the East Antarctic ice sheet: A new view of the Wilkes Subglacial Basin. *Tectonophysics*, 478(1), 62–77. https://doi.org/10.1016/j.tecto.2009.03.013
- Ferraccioli, F., Corr, H., Jordan, T., Robinson, C., Armadillo, E., Bozzo, E., & Caneva, G. (2021). Processed airborne radio-echo sounding data from the WISE-ISODYN survey across the Wilkes Subglacial Basin, East Antarctica (2005/2006) (1.0, p. 288 files, 58.7 GB) [Application/octet-stream,SEG-Y,application/x-hdf,application/pdf]. NERC EDS UK Polar Data Centre. https://doi.org/10.5285/70ADAB3D-3632-400D-9AA1-DDF2D62A11B3
- Hale, R., Miller, H., Gogineni, S., Yan, J. B., Rodriguez-Morales, F., Leuschen, C., et al. (2016). Multi-channel ultra-wideband radar sounder and imager. In 2016 IEEE international geoscience and remote sensing symposium (IGARSS) (pp. 2112–2115). https://doi.org/10.1109/ IGARSS.2016.7729545
- Haynes, M. S., Chapin, E., & Schroeder, D. M. (2018). Geometric power fall-off in radar sounding. IEEE Transactions on Geoscience and Remote Sensing, 56(11), 6571–6585. https://doi.org/10.1109/TGRS.2018.2840511
- Heliere, F., Lin, C.-C., Corr, H., & Vaughan, D. (2007). Radio echo sounding of Pine Island Glacier, West Antarctica: Aperture synthesis processing and analysis of feasibility from space. *IEEE Transactions on Geoscience and Remote Sensing*, 45(8), 2573–2582. https://doi.org/10.1109/TGRS.2007.897433
- Hills, B. H., Christianson, K., & Holschuh, N. (2020). A framework for attenuation method selection evaluated with ice-penetrating radar data at South Pole Lake. *Annals of Glaciology*, 61(81), 176–187. https://doi.org/10.1017/aog.2020.32
- Jacobel, R. W., Lapo, K. E., Stamp, J. R., Youngblood, B. W., Welch, B. C., & Bamber, J. L. (2010). A comparison of basal reflectivity and ice velocity in East Antarctica. The Cryosphere, 4(4), 447–452. https://doi.org/10.5194/tc-4-447-2010
- Jordan, J. R., Miles, B. W. J., Gudmundsson, G. H., Jamieson, S. S. R., Jenkins, A., & Stokes, C. R. (2023). Increased warm water intrusions could cause mass loss in East Antarctica during the next 200 years. *Nature Communications*, 14(1), 1825. https://doi.org/10.1038/s41467-023-37553-2
- Jordan, T. M., Bamber, J. L., Williams, C. N., Paden, J. D., Siegert, M. J., Huybrechts, P., et al. (2016). An ice-sheet-wide framework for englacial attenuation from ice-penetrating radar data. The Cryosphere, 10(4), 1547–1570. https://doi.org/10.5194/tc-10-1547-2016
- Kleiner, T., & Humbert, A. (2014). Numerical simulations of major ice streams in Western Dronning Maud Land, Antarctica, under wet and dry basal conditions. *Journal of Glaciology*, 60(220), 215–232. https://doi.org/10.3189/2014JoG13J006
- Kyrke-Smith, T. M., Katz, R. F., & Fowler, A. C. (2014). Subglacial hydrology and the formation of ice streams. Proceedings of the Royal Society A: Mathematical, Physical and Engineering Sciences, 470(2161), 20130494. https://doi.org/10.1098/rspa.2013.0494
- Lovell, A. M., Stokes, C. R., & Jamieson, S. S. R. (2017). Sub-decadal variations in outlet glacier terminus positions in Victoria Land, Oates Land and George V Land, East Antarctica (1972–2013). Antarctic Science, 29(5), 468–483. https://doi.org/10.1017/S0954102017000074
- MacGregor, J. A., Li, J., Paden, J. D., Catania, G. A., Clow, G. D., Fahnestock, M. A., et al. (2015). Radar attenuation and temperature within the Greenland ice sheet. *Journal of Geophysical Research: Earth Surface*, 120(6), 983–1008. https://doi.org/10.1002/2014JF003418
- Mantelli, E., Haseloff, M., & Schoof, C. (2019). Ice sheet flow with thermally activated sliding. Part 1: The role of advection. *Proceedings of the Royal Society A: Mathematical, Physical and Engineering Sciences*, 475(2230), 20190410. https://doi.org/10.1098/rspa.2019.0410
- Mantelli, E., & Schoof, C. (2019). Ice sheet flow with thermally activated sliding. Part 2: The stability of subtemperate regions. Proceedings of the Royal Society A: Mathematical, Physical and Engineering Sciences, 475(2231), 20190411. https://doi.org/10.1098/rspa.2019.0411
- Matsuoka, K., MacGregor, J. A., & Pattyn, F. (2012). Predicting radar attenuation within the Antarctic ice sheet. *Earth and Planetary Science Letters*, 359(360), 173–183. https://doi.org/10.1016/j.epsl.2012.10.018
- Matsuoka, K., Pattyn, F., Callens, D., & Conway, H. (2012). Radar characterization of the basal interface across the grounding zone of an ice-rise promontory in East Antarctica. *Annals of Glaciology*, 53(60), 29–34. https://doi.org/10.3189/2012AoG60A106
- McCullagh, P., & Nelder, J. A. (1989). Generalized linear models (2nd ed.). Chapman and Hall.
- Mengel, M., & Levermann, A. (2014). Ice plug prevents irreversible discharge from East Antarctica. Nature Climate Change, 4(6), 451–455. https://doi.org/10.1038/nclimate2226
- Mercer, J. H. (1978). West Antarctic ice sheet and CO₂ greenhouse effect: A threat of disaster. Nature, 271(5643), 321–325. Article 5643. https://doi.org/10.1038/271321a0
- Miles, B. W. J., Stokes, C. R., & Jamieson, S. S. R. (2018). Velocity increases at Cook Glacier, East Antarctica, linked to ice shelf loss and a subglacial flood event. The Cryosphere, 12(10), 3123–3136. https://doi.org/10.5194/tc-12-3123-2018
- Morlighem, M. (2022). MEaSUREs BedMachine Antarctica, version 3 [Dataset]. NASA National Snow and Ice Data Center Distributed Active Archive Center. https://doi.org/10.5067/FPSU0V1MWUB6
- Morlighem, M., Rignot, E., Binder, T., Blankenship, D., Drews, R., Eagles, G., et al. (2020). Deep glacial troughs and stabilizing ridges unveiled beneath the margins of the Antarctic ice sheet. *Nature Geoscience*, 13(2), 132–137. https://doi.org/10.1038/s41561-019-0510-8
- Mouginot, J., Scheuchl, B., & Rignot, E. (2012). Mapping of ice motion in Antarctica using synthetic-aperture radar data. *Remote Sensing*, 4(9), 2753–2767. Article 9. https://doi.org/10.3390/rs4092753
- Oswald, G. K. A., & Gogineni, S. P. (2012). Mapping basal melt under the northern Greenland Ice Sheet. *IEEE Transactions on Geoscience and Remote Sensing*, 50(2), 585–592. https://doi.org/10.1109/TGRS.2011.2162072
- Pattyn, F. (2010). Antarctic subglacial conditions inferred from a hybrid ice sheet/ice stream model. Earth and Planetary Science Letters, 295(3–4), 451–461. https://doi.org/10.1016/j.epsl.2010.04.025
- Peters, M. E., Blankenship, D. D., Carter, S. P., Kempf, S. D., Young, D. A., & Holt, J. W. (2007). Along-track focusing of airborne radar sounding data from West Antarctica for improving basal reflection analysis and layer detection. *IEEE Transactions on Geoscience and Remote Sensing*, 45(9), 2725–2736. https://doi.org/10.1109/TGRS.2007.897416

DAWSON ET AL. 11 of 12

- Peters, M. E., Blankenship, D. D., & Morse, D. L. (2005). Analysis techniques for coherent airborne radar sounding: Application to West Antarctic ice streams. *Journal of Geophysical Research*, 110(B6), B06303. https://doi.org/10.1029/2004JB003222
- Pittard, M. L., Whitehouse, P. L., Bentley, M. J., & Small, D. (2022). An ensemble of Antarctic deglacial simulations constrained by geological observations. *Quaternary Science Reviews*, 298, 107800. https://doi.org/10.1016/j.quascirev.2022.107800
- Pollard, D., Chang, W., Haran, M., Applegate, P., & DeConto, R. (2016). Large ensemble modeling of the last deglacial retreat of the West Antarctic Ice Sheet: Comparison of simple and advanced statistical techniques. Geoscientific Model Development, 9(5), 1697–1723. https://doi.org/10.5194/gmd-9-1697-2016
- Reese, R., Levermann, A., Albrecht, T., Seroussi, H., & Winkelmann, R. (2020). The role of history and strength of the oceanic forcing in sea level projections from Antarctica with the Parallel Ice Sheet Model. *The Cryosphere*, 14(9), 3097–3110. https://doi.org/10.5194/tc-14-3097-2020 Rignot, E., Mouginot, J., & Scheuchl, B. (2011). Ice flow of the Antarctic ice sheet. *Science*, 333(6048), 1427–1430. https://doi.org/10.1126/
- Rignot, E., Mouginot, J., Scheuchl, B., van den Broeke, M., van Wessem, M. J., & Morlighem, M. (2019). Four decades of Antarctic ice sheet mass balance from 1979–2017. Proceedings of the National Academy of Sciences, 116(4), 1095–1103. https://doi.org/10.1073/pnas.1812883116
- Rignot, E. J., Mouginot, J., & Scheuchl, B. (2017). MEaSUREs InSAR-based Antarctica ice velocity map, version 2 [Dataset]. NASA National Snow and Ice Data Center Distributed Active Archive Center. https://doi.org/10.5067/D7GK8F5J8M8R
- Scambos, T. A., Bell, R. E., Alley, R. B., Anandakrishnan, S., Bromwich, D. H., Brunt, K., et al. (2017). How much, how fast? A science review and outlook for research on the instability of Antarctica's Thwaites Glacier in the 21st century. *Global and Planetary Change*, 153, 16–34. https://doi.org/10.1016/j.gloplacha.2017.04.008
- Schlegel, R., Kulessa, B., Murray, T., & Eisen, O. (2023). Towards a common terminology in radioglaciology. Annals of Glaciology, 63(87–89), 1–5. https://doi.org/10.1017/aog.2023.2
- Schoof, C. (2007). Ice sheet grounding line dynamics: Steady states, stability, and hysteresis. *Journal of Geophysical Research*, 112(F3), F03S28. https://doi.org/10.1029/2006JF000664
- Schröder, L., Horwath, M., Dietrich, R., Helm, V., van den Broeke, M. R., & Ligtenberg, S. R. M. (2019). Four decades of Antarctic surface elevation changes from multi-mission satellite altimetry. *The Cryosphere*, 13(2), 427–449. https://doi.org/10.5194/tc-13-427-2019
- Schroeder, D. M., Bingham, R. G., Blankenship, D. D., Christianson, K., Eisen, O., Flowers, G. E., et al. (2020). Five decades of radioglaciology. Annals of Glaciology, 61(81), 1–13. https://doi.org/10.1017/aog.2020.11
- Schroeder, D. M., Seroussi, H., Chu, W., & Young, D. A. (2016). Adaptively constraining radar attenuation and temperature across the Thwaites Glacier catchment using bed echoes. *Journal of Glaciology*, 62(236), 1075–1082. https://doi.org/10.1017/jog.2016.100
- Seroussi, H. (2019). Results of the initMIP-Antarctica experiments: An ice sheet initialization intercomparison of ISMIP6 [Dataset]. Zenodo. https://doi.org/10.5281/zenodo.2651652
- Seroussi, H., Ivins, E. R., Wiens, D. A., & Bondzio, J. (2017). Influence of a West Antarctic mantle plume on ice sheet basal conditions. *Journal of Geophysical Research: Solid Earth*, 122(9), 7127–7155. https://doi.org/10.1002/2017JB014423
- Seroussi, H., Nowicki, S., Payne, A. J., Goelzer, H., Lipscomb, W. H., Abe-Ouchi, A., et al. (2020). ISMIP6 Antarctica: A multi-model ensemble of the Antarctic ice sheet evolution over the 21st century. *The Cryosphere*, 14(9), 3033–3070. https://doi.org/10.5194/tc-14-3033-2020
- Siegert, M. J., & Glasser, N. F. (1997). Convergent flow of ice within the Astrolabe subglacial basin, Terre Adélie, East Antarctica: An hypothesis
- derived from numerical modelling experiments. *Polar Research*, 16(1), 63–72. Article 1. https://doi.org/10.3402/polar.v16i1.6625
 Stokes, C. R., Abram, N. J., Bentley, M. J., Edwards, T. L., England, M. H., Foppert, A., et al. (2022). Response of the East Antarctic ice sheet to past and future climate change. *Nature*, 608(7922), 275–286. Article 7922. https://doi.org/10.1038/s41586-022-04946-0
- The IMBIE team. (2018). Mass balance of the Antarctic ice sheet from 1992 to 2017. *Nature*, 558(7709), 219–222. https://doi.org/10.1038/s41586-018-0179-y
- Thompson, A. F., Stewart, A. L., Spence, P., & Heywood, K. J. (2018). The Antarctic slope current in a changing climate. *Reviews of Geophysics*, 56(4), 741–770. https://doi.org/10.1029/2018RG000624
- Wilch, E., & Hughes, T. J. (2000). Calculating basal thermal zones beneath the Antarctic ice sheet. *Journal of Glaciology*, 46(153), 297–310. https://doi.org/10.3189/172756500781832927

DAWSON ET AL. 12 of 12